ACS Sustainable Chemistry & Engineering

Research Article

pubs.acs.org/journal/ascecg

Toward Sustainable Chemoselective Nitroarene Hydrogenation Using Supported Gold as Catalyst

Xiaodong Wang, Fernando Cárdenas-Lizana, and Mark A. Keane*

Chemical Engineering, School of Engineering and Physical Sciences, Heriot-Watt University, Edinburgh EH14 4AS, Scotland

ABSTRACT: We have taken a systematic approach to the clean production of functionalized aromatic amines, adopting the hydrogenation of *o*-chloronitrobenzene (*o*-CNB) to *o*-chloroaniline (*o*-CAN) as a case study. We tested a laboratory-synthesized Au/TiO_2 catalyst against a commercial benchmark (Pd/C). Both catalysts exhibited nanoscale (1−9 nm)-supported metal particles (d_{TEM} = 4.0 nm (Au) and 5.4 nm (Pd)). In batch liquid phase operation, Pd/C was nonselective, generating aniline and nitrobenzene as undesired byproducts, where elevated P_{H_2} (5−12 atm) increased the rate and *o*-CAN selectivity (to 86%). In contrast, Au/TiO_2 promoted exclusive *o*-CAN production regardless of P_{H_2} but at a lower rate. Reaction exclusivity extended to (ambient pressure) gas phase continuous processing with 100% *o*-CAN yield and catalyst stability up to 140 h on-stream. A switch from batch to continuous operation was accompanied by an increase in projected *o*-CAN production capacity ($5 \times 10^3 \rightarrow 86 \times 10^3$ $kg_{o\text{-CAN}}$ kg_{Au}^{-1} $year^{-1}$). Water (as *o*-CNB carrier) served as an additional source of reactive hydrogen to deliver an order of magnitude increase in the selective hydrogenation rate (vs ethanol) and a production capacity of 14×10^5 $kg_{o\text{-CAN}}$ kg_{Au}^{-1} $year^{-1}$. Our ultimate catalytic process explicitly addresses nine of the 12 green chemistry principles with an E-factor = 0.28.

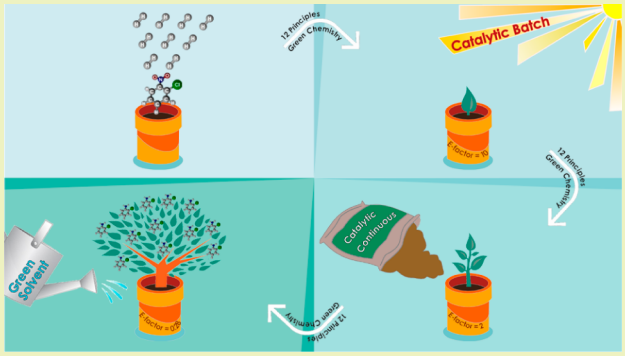

KEYWORDS: *Sustainable processing, Green chemistry principles, E-factor, Chloronitrobenzene, Chloroaniline, Gold catalysis*

INTRODUCTION

Sustainability is a crucial issue facing the chemical sector, where the application of catalysis to reduce energy requirements and achieve high selectivities is key to the application of "green chemistry".[1] Several metrics have emerged to quantify green performance, notably the environmental factor (E-factor, kg_{waste} $kg_{product}^{-1}$) and derivatives (e.g., process mass intensity (PMI) = E-factor + 1).[2] E-factor values within the 1−5 range are characteristic of highly optimized processes[3] in the manufacture of pharmaceuticals, dyes, and fine chemicals industries.[4] The attainment of a sustainable chemical process should draw on the 12 principles of green chemistry,[5−7] summarized in Table 1. In this study, we have set out to develop a low energy, atom efficient, continuous process for the production of functionalized amines (used in the manufacture of agrochemicals, pharmaceuticals, dyes, and pigments[8]), taking the hydrogenation of *o*-chloronitrobenzene (*o*-CNB) to *o*-chloroaniline (*o*-CAN) as a model reaction.

The conventional route to haloamines via reduction of the corresponding nitro-compound by an Fe-promoted reaction in acid media (Béchamp process) delivers low product yields and generates significant quantities of toxic Fe/FeO sludge waste[9] with an associated E-factor = 15.[10] To date, CNB hydrogenation has focused on batch liquid phase operation using pressurized (up to 40 atm) hydrogen.[11,12] A range of volatile organic solvents (methanol,[13] ethanol,[14] diethyl ether,[13] and toluene[15]) have been employed with serious implications in terms of safety (flammability) and environmental impact (toxic emissions). Incomplete mixing in batch reactors results in significant mass/heat transfer gradients, leading to byproduct formation with the requirement for separation/purification stages to extract the target product.[16] A switch to continuous gas phase operation offers clear advantages in circumventing "down time" between batches, while operation at atmospheric H_2 reduces safety risks in terms of gas leakage and explosion.[17] In continuous operation, reactant/catalyst contact time can be adjusted to tune selectivity.[8] A number of catalytic metals (e.g., Pt, Ru, Ni)[9] have been tested in CNB hydrogenation where high selectivities to the target amine (up to 100%) have been achieved over supported Au[18] and Pd[19] in the gas[18] and liquid[18,19] phases. There is however a dearth of literature that has compared catalytic action in both batch liquid and continuous gas operation. In this work, we apply the green chemistry principles as a roadmap to maximize process efficiency in the hydrogenation of *o*-CNB to *o*-CAN over Au/TiO_2, taking Pd/C as a benchmark and employing the E-factor as a measure of environmental performance.

Received: August 22, 2014
Revised: October 9, 2014
Published: October 17, 2014

   dx.doi.org/10.1021/sc500544s | ACS Sustainable Chem. Eng. 2014, 2, 2781−2789

Table 1. Roadmap of Steps Considered in This Work To Implement Sustainable Hydrogenation of *o*-CNB (to *o*-CAN) (right) According to the 12 Principles of Green Chemistry[5,6] (left), Using the E-factor as the Guiding Metric.[2]

Principles of Green Chemistry	
No.	**Descriptor**
1	Waste prevention
2	Atom economy
3	Safer synthesis
4	Safer products by design
5	Safer auxiliaries
6	Energy efficiency
7	Renewable feedstocks
8	Reduce derivatives
9	Catalysis
10	Degradability
11	Pollution prevention
12	Accident prevention

Steps considered to Implement Sustainability				
Step	**Reaction System**	**Principle number(s)**	**E-factor / Improvement achieved**	**Issue tackled in next step**
	Béchamp process	9	15[a] / -	Catalytic instead of stoichiometric reagents
I	Pd/C P_{H_2} = 12 atm Batch liquid Solvent = Ethanol	1 2 10 11	10[b] / Catalytic route	No by-products (*i.e.* NB and AN)
II	Au/TiO_2 P_{H_2} = 12 atm Batch liquid Solvent = Ethanol	3 6 12	8[b] / 100% selectivity, no *by*-products	Batch operation at high pressure (P_{H_2} = 12 atm)
III	Au/TiO_2 P_{H_2} = 1 atm Continuous gas Solvent = Ethanol	1 2 5 6 11 12	8[b] / Reaction at P_{H_2} = 1 atm	Organic (ethanol) solvent
IV	Au/TiO_2 P_{H_2} = 1 atm Continuous gas Solvent = H_2O		0.28[b] / Green solvent (H_2O)	

[a]E-factor extracted from ref 10 for industrial scale nitroarene reduction. [b]Calculated E-factor considering 90% recovery of ethanol or water (solvent).[7]

EXPERIMENTAL SECTION

Catalyst Preparation and Activation. The TiO_2 support (P25, Degussa) was used as received. The 0.1% w/w Au/TiO_2 was prepared by deposition−precipitation following the synthesis procedure described in detail elsewhere.[20] Urea (as basification agent) was added (about 100-fold excess) to a $HAuCl_4$ solution (5×10^{-4} M) containing the TiO_2 support, and the suspension was stirred and heated to 353 K for 3 h. The pH progressively increased to reach about 7 as a result of thermally induced urea decomposition. The solid obtained was separated by centrifugation, washed with deionized water (with centrifugation between each washing) until chlorine free (confirmed by the $AgNO_3$ test), and dried under He (45 cm^3 min^{-1}) at 373 K (2 K min^{-1}) for 5 h. Prior to use in catalysis, the sample (75 μm average diameter) was activated in 60 cm^3 min^{-1} H_2 at 2 K min^{-1} to 473 K. A commercial 10% w/w Pd/C catalyst (Aldrich) activated at 573 K (10 K min^{-1}) in H_2 was tested as the benchmark. After activation, the samples were passivated in 1% v/v O_2/He at ambient temperature for off-line characterization.

Catalyst Characterization. Metal (Au and Pd) loading was determined by inductively coupled plasma-optical emission spectrometry (ICP-OES, Vista-PRO, Varian, Inc.). Nitrogen adsorption−desorption isotherms were obtained at 77 K on the automated Micromeritics Gemini 2390 system. Specific surface areas (SSA) were calculated using the standard BET method. Total pore volume was obtained at a relative N_2 pressure (P/P_0) = 0.95; samples were outgassed at 423 K for 1 h prior to analysis. Temperature-programmed reduction (TPR) and H_2 chemisorption were determined using the CHEM-BET 3000 (Quantachrome) unit. The samples were heated in 17 cm^3 min^{-1} 5% v/v H_2/N_2 at 2−10 K min^{-1} to 473−573 K. The effluent gas passed through a liquid N_2 trap, and changes in H_2 consumption were monitored by TCD with acquisition/manipulation using the TPR Win software. The reduced samples were swept with 65 cm^3 min^{-1} N_2 for 1.5 h, cooled to reaction (423 K) or ambient (298 K) temperature, and subjected to H_2 chemisorption ($P = 1.5 \times 10^{-4}$ atm) using pulse (10−50 μL) titration. SSA and H_2 chemisorption values were reproducible to within ±5%, and values quoted represent the mean. Powder X-ray diffractograms were recorded on a Bruker/Siemens D500 incident X-ray diffractometer using Cu Kα radiation; samples were scanned (0.02° $step^{-1}$) over the range of $20° \leq 2\theta \leq 85°$. Metal particle morphology was determined by TEM analysis; a JEOL JEM 2011 HRTEM unit operated at an accelerating voltage of 200 kV using Gatan DigitalMicrograph 3.4 was used for data analysis. Samples were dispersed in acetone and deposited on a holey carbon/Cu grid (300 Mesh). Surface area-weighted metal diameter (d_{TEM}) was calculated (a count of 200 Au and 580 Pd particles) from

$$d_{TEM} = \frac{\sum_i n_i d_i^3}{\sum_i n_i d_i^2} \quad (1)$$

where n_i is the number of particles of diameter d_i.

Catalytic Systems. *Materials and Analytical Methods.* Reactant (*o*-CNB, Sigma-Aldrich, ≥98%) and solvent (ethanol, Sigma-Aldrich, ≥99%) were used as received. Gases (H_2, He, O_2, and N_2) were ultrahigh purity (99.999%, BOC). Product composition was determined by capillary GC (PerkinElmer Auto System XL with flame ionization detector) using a DB-1 capillary column (J&W Scientific); carbon mass balance was complete to ±5%. Repeated reactions delivered conversion/selectivity values reproducible to better than ±5%.

Liquid Phase Batch Operation. Reactions (T = 423 K; P_{H_2} = 5−12 atm; P_{total} = 13−20 atm) were conducted in a commercial semibatch

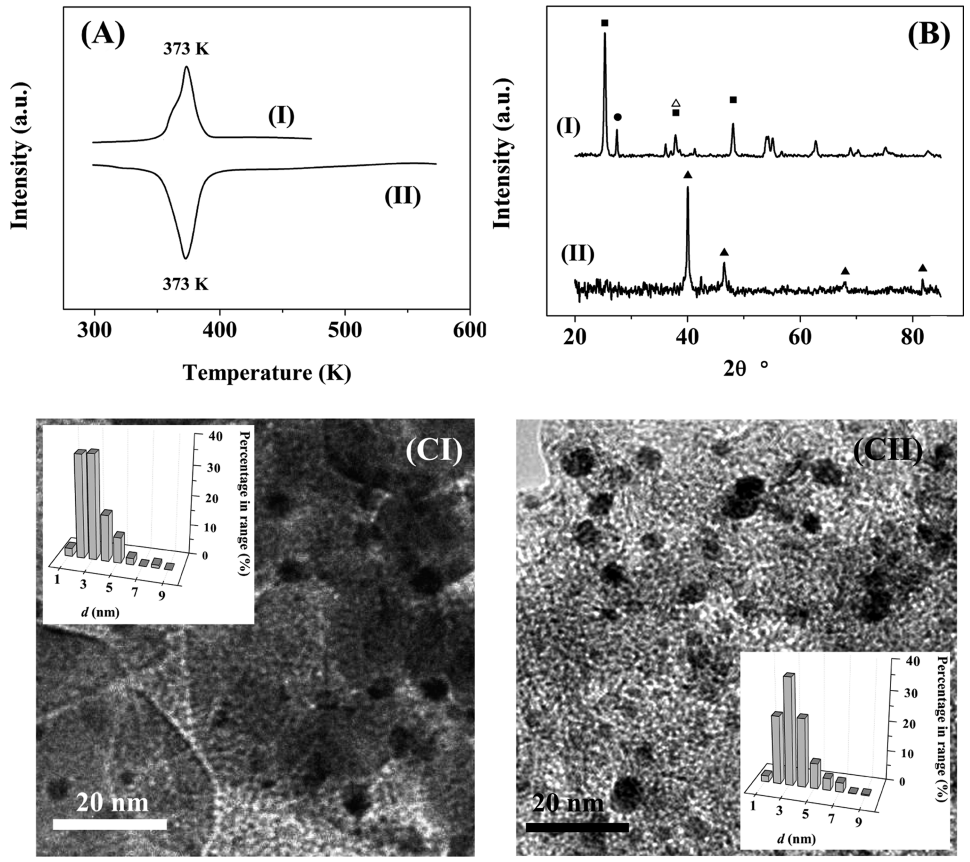

Figure 1. (A) TPR profiles, (B) XRD patterns (TiO_2—anatase (21—1272), ■; TiO_2—rutile (21—1276), ●; Au (04—0784), △; Pd (05—0681), ▲), and (C) representative TEM images with associated (inset) metal particle size distribution histograms for (I) Au/TiO_2 and (II) Pd/C.

stirred stainless steel reactor (100 cm^3 autoclave, Büchi) equipped with a pressure-controlled H_2 supply. Adopting the approach of Madon and Boudart,[21] the reaction operational window was established to ensure minimal heat or mass transfer limitations. Hydrogen consumption during reaction was monitored online with a press flow gas controller (BPC-6002, Büchi) and a stainless steel six-blade disk turbine impeller provided effective agitation (1800 rpm). A recirculator (HAAKE B-N3) was used to control the reaction temperature to ±1 K. At the beginning of each run, an 80 cm^3 ethanolic solution ($0.3 \times 10^{-2} - 6.4 \times 10^{-2}$ mol dm^{-3}) of *o*-CNB was charged and flushed three times with N_2 under constant agitation. The catalyst was activated ex situ, transferred to the reactor, and the temperature stabilized under gentle stirring (about 300 rpm). Hydrogen was introduced, the system pressurized to the final reaction pressure, and full agitation engaged (time t = 0 for reaction). In a series of blank tests, reaction in the absence of catalyst did not result in measurable conversion. The initial molar *o*-CNB/metal (Au or Pd) = 250—3300. Noninvasive liquid sampling via a syringe with in-line filters allowed controlled removal of aliquots (≤0.5 cm^3) from the reactor for analysis. Fractional conversion of *o*-CNB (x) is defined as

$$x(-) = \frac{C_{o\text{-CNB},0} - C_{o\text{-CNB}}}{C_{o\text{-CNB},0}} \quad (2)$$

where subindex "0" refers to initial concentration. Initial *o*-CNB consumption rate (r) was determined from a linear regression of the temporal *o*-CNB concentration profiles at $x < 0.25$.[22] Selectivity (%) to target *o*-CAN ($S_{o\text{-CAN}}$) is given by

$$S_{o\text{-CAN}} = \frac{C_{o\text{-CAN}}}{C_{o\text{-CNB},0} - C_{o\text{-CNB}}} \times 100 \quad (3)$$

Continuous Gas Phase Operation. Reactions were carried out under atmospheric pressure in a fixed bed vertical continuous flow glass reactor (i.d. = 15 mm) at 423 K under conditions of negligible heat/mass transport limitations. Isothermal conditions (±1 K) were maintained by thoroughly mixing the catalyst with ground glass (75 μm). An ethanolic (or aqueous) *o*-CNB solution ($F = 6 \times 10^{-3} - 0.76$ mmol h^{-1}; molar metal to inlet *o*-CNB = $0.03 \times 10^{-2} - 0.34$ h) was delivered, in a concurrent flow of H_2 (GHSV = 2×10^4 h^{-1}) via a glass/Teflon airtight syringe and Teflon line using a microprocessor controlled infusion pump (Model 100 kd Scientific) at a fixed calibrated flow rate. In blank tests, passage of *o*-CNB in H_2 through the empty reactor did not result in detectable conversion. Fractional hydrogenation (x) was obtained from

$$x(-) = \frac{C_{o\text{-CNB,in}} - C_{o\text{-CNB,out}}}{C_{o\text{-CNB,in}}} \quad (4)$$

where "in" and "out" refer to the inlet and outlet streams. Selectivity is given by

$$S_{o\text{-CAN}} = \frac{C_{o\text{-CAN,out}}}{C_{o\text{-CNB,in}} - C_{o\text{-CNB,out}}} \times 100 \quad (5)$$

RESULTS AND DISCUSSION

Catalyst Characteristics. TPR (to 473 K) of the TiO_2 support (profile not shown) did not result in any measurable H_2 consumption. This is consistent with the literature[23] where TiO_2 reduction (in H_2) required temperatures in excess of 773 K.[24,25] Hydrogen consumption with a temperature maximum (T_{max}) at 373 K was recorded in the TPR of Au/TiO_2 (Figure 1(A,I)). A single positive TPR peak has been reported elsewhere for Au/TiO_2 with T_{max} at 378[26] and 383 K.[27] The H_2 consumed (9.2 mmol g_{Au}^{-1}) was measurably higher than that (7.6 mmol g_{Au}^{-1}) required for $Au^{3+} \rightarrow Au^0$ reduction,

dx.doi.org/10.1021/sc500544s | ACS Sustainable Chem. Eng. 2014, 2, 2781—2789

suggesting partial (surface) reduction of TiO_2 with the creation of oxygen vacancies.[28] This is significant as surface vacancies formed during the reduction of Ni/TiO_2 served to activate N═O for reaction.[29] We accordingly adopted a reduction temperature of 473 K for the activation of Au/TiO_2 prior to catalysis. The SSA of Au/TiO_2 matched that of the starting TiO_2, but there was a measurable increase in pore volume (Table 2) that has been observed previously.[30]

Table 2. Physicochemical Characteristics of Au/TiO_2 and Pd/C

	Au/TiO_2	Pd/C
TPR T_{max} (K)	373	373[a]
SSA ($m^2\ g^{-1}$)	48 (49)[b]	826
total pore volume ($cm^3\ g^{-1}$)	0.13 (0.07)[b]	0.37
H_2 chemisorption ($\mu mol\ g^{-1}$)	20[c]/183[d]	1691[c]/637[d]
metal particle size range (nm)	1−8	1−9
average particle size (nm)	4.0[e]	5.4[e]/6.1[f]/4.7[g]

[a]Negative peak due to the decomposition of β-Pd hydride. [b]Value refers to TiO_2 (support). [c]Measurements conducted at 298 K. [d]Measurements conducted at 423 K. [e]From TEM analysis (see eq 1). [f]From XRD measurements. [g]From H_2 chemisorption (at 298 K).

The XRD pattern (Figure 1(B,I)) for Au/TiO_2 is characterized by peaks at 2θ = 25.3°, 37.8°, and 48.1° corresponding to the (101), (004), and (200) planes of tetragonal anatase (JCPDS-ICDD 21-1272), while the peak at 27.4° is diagnostic of tetragonal rutile (JCPDS-ICDD 21-1276). The anatase content from the XRD response was close to the 80% volume fraction reported for Degussa P25.[31] There were no strong signals detected for Au metal (principal peak at 38.1°), which may be due to the low Au loading (0.1% w/w) and/or occurrence of a well-dispersed Au phase (<5 nm).[32] The latter was confirmed by TEM, which revealed pseudospherical Au particles in the size range 1−8 nm (Figure 1(C,I)) with a surface area-weighted mean diameter of 4.0 nm. The formation of supported Au particles at the nanoscale (<10 nm) is critical for hydrogenation activity.[18] It is established that Au exhibits a higher barrier than other transition metals (Pt, Pd, and Ni) for H_2 dissociation due to the filled *d*-band, and chemisorption proceeds at edge and corner sites associated with smaller particles.[33,34] We have demonstrated previously that the specific rate of nitro-compound (nitrocyclohexane,[28] *p*-CNB,[35] and *m*-dinitrobenzene (*m*-DNB)[36]) reduction increased with decreasing mean Au size (from 9 to 3 nm). Ambient temperature H_2 chemisorption following TPR delivered an appreciably lower uptake (20 $\mu mol\ g^{-1}$) than that (183 $\mu mol\ g^{-1}$) recorded at reaction temperature (423 K, Table 2), indicating that H_2 adsorption on Au is an activated process, as noted by Bus et al.[34] and Lin and Vannice.[37]

Critical physicochemical characteristics for the Pd/C catalyst are presented in Figure 1 and Table 2. The SSA (826 $m^2\ g^{-1}$) and pore volume (0.37 $cm^3\ g^{-1}$) are close to those (875 $m^2\ g^{-1}$; 0.47 $cm^3\ g^{-1}$) reported elsewhere[38] for activated carbon-supported Pd. TPR analysis (to 573 K) generated a single negative peak with T_{max} = 373 K (Figure 1(A,II)) that can be attributed to H_2 generated from the thermal decomposition of the β−Pd hydride. Zero valent Pd can absorb H_2 at ambient temperature[39] to form a hydride where the H_2 partial pressure > 0.02 atm;[40] a pressure of 0.05 atm was used in this study. This hydride decomposes at 340−390 K[22,41] with a H_2 release that is dependent on Pd size with an upper limit of 0.67 $mol_H\ mol_{Pd}^{-1}$ for bulk Pd,[42] decreasing to about 0.05 $mol_H\ mol_{Pd}^{-1}$ for a mean Pd size of about 2 nm.[42] The value recorded in this study (0.16 $mol_H\ mol_{Pd}^{-1}$) suggests formation of Pd particles at the nanoscale, as confirmed by TEM analysis (Figure 1(C,II)) with a size distribution in the 1−9 nm range and mean of 5.4 nm. The XRD pattern (Figure 1(B,II)) exhibits signals at 40.7°, 46.1°, 68.1°, and 82.1° that can be assigned to Pd (111), (200), (220), and (311) planes, respectively. A Pd particle size of 6.1 nm was obtained by applying standard line broadening analysis.[43] Ambient temperature H_2 chemisorption (1691 $\mu mol\ g^{-1}$) far exceeded that measured for Au/TiO_2 (Table

Table 3. Comparison of Batch Liquid (at different P_{H_2}) vs Continuous Gas Phase Operation in Terms of Process Parameters and Ultimate *o*-CAN Production Capacity over Pd/C and Au/TiO_2

Step	Catalyst	Operation Mode	Solvent	P_{H_2} (atm)	r[a]	$S_{o\text{-}CAN}/S_{AN}/S_{NB}$ (%)	Down time[b] steps (h)	Production capacity[c]
I	Pd/C	Batch Liquid	Ethanol	5	2290	79/20/1		
				8	2470	79/20/1		
				10	2650	81/18/1		
				12	2910	86/13/1		
II	Au/TiO_2			5	10	100/0/0	$t_1+t_2+t_3+t_4+t_5$ = 10	5×10^3
				8	40			
				10	58			
				12	167			
III		Continuous Gas		1	12		$t_1+t_2+t_3$ = 3	86×10^3
IV			H_2O		200			14×10^5

[a]$mol_{o\text{-}CNB}\ mol_{metal}^{-1}\ h^{-1}$. [b]Time required for reactor loading (t_1), catalyst activation (t_2), temperature/pressure stabilization (t_3), unload/reload of product/reactant solution (t_4), and catalyst filtration-washing-reloading (t_5). [c]$kg_{o\text{-}CAN}\ kg_{Au}^{-1}\ year^{-1}$

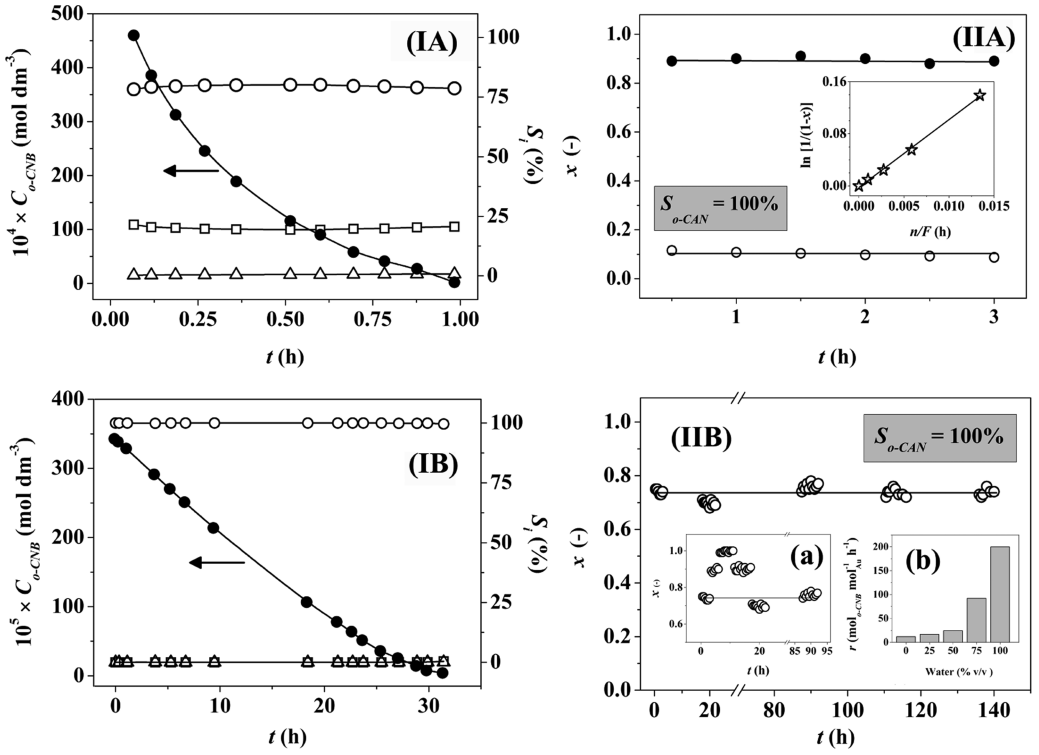

Figure 2. (I) Batch liquid phase reaction: temporal variation of *o*-CNB concentration ($C_{o\text{-CNB}}$: ●) and product selectivity (S_i: *o*-CAN, ○; AN, □; NB, △) for the reaction over (A) Pd/C and (B) Au/TiO_2. Reaction conditions: $C_{o\text{-CNB},0}$/Pd molar ratio = 3300, $C_{o\text{-CNB},0}$/Au molar ratio = 250, T = 423 K, P_{H_2} = 5 atm. (II) Continuous gas phase reaction: (A) variation of *o*-CNB fractional conversion (x) with time on-stream for reaction over Au/TiO_2 at $n/F = 12 \times 10^{-3}$ h (○) and 16×10^{-2} h (●). Inset: pseudo-first-order kinetic plot; (B) fractional conversion over Au/TiO_2 for up to 140 h on-stream ($n/F = 8 \times 10^{-2}$ h). Insets: (a) fractional conversion over Au/TiO_2 for up to 95 h on-stream with a switch in n/F (from 8×10^{-2} h to 34×10^{-2} h) between 3 and 17 h. Reaction conditions: T = 423 K, P_{H_2} = 1 atm and (b) variation of hydrogenation rate (r) with water content (% v/v) in the carrier (water and water + ethanol mixtures).

2). Hydrogen adsorption on supported Pd is a valid means of estimating Pd particle size,[44] where the value (4.7 nm) obtained (adopting a Pd/H adsorption stoichiometry = 1) is consistent with that determined by TEM and/or XRD. Hydrogen chemisorption on Pd/C was lower (637 μmol g^{-1}) at the reaction temperature but was still significantly greater than that recorded for Au/TiO_2. Our results are consistent with the work of Greeley and Mavrikakis[45] who demonstrated by DFT that Au weakly binds hydrogen relative to Pd. The same authors showed that hydrogen uptake on Pd is exothermic, which can account for lower adsorption at increased temperature.

o-CNB Hydrogenation. In this work, we have set out to systematically evaluate and tackle the major sustainability issues associated with the production of *o*-CAN (from *o*-CNB) using the 12 principles of green chemistry to minimize E-factor and maximize productivity. We present the reaction systems considered in this work in Table 1 wherein we identify the associated drawbacks and steps taken to circumvent these limitations.

First Approach to Optimisation: Batch Liquid Phase Operation over Pd/C. In addition to the target *o*-CAN, a range of byproducts have been identified in the literature for the hydrogenation of *o*-CNB in gas[9,46,47] and liquid[9,15,48] phase operation. Nitrobenzene (NB) and aniline (AN) are produced via hydrodechlorination of *o*-CNB with further hydrogenation, as observed over NiCoB[49] and Pt/C.[50] Hydrodeamination to chlorobenzene has been reported for Pt/Al_2O_3,[51] while benzene formation over Ru catalysts has been noted by Xiao et al.[9] Nitrosochloro- and (chlorophenyl)-hydroxylamine intermediates can undergo side (condensation/hydrogenation) reactions with *o*-CAN to generate toxic byproducts (dichloroazobenzene, dichlorohydrazobenzene, and/or dichloroazoxybenzene), which have been isolated over Pt powders.[48] Conventional synthesis of *o*-CAN by the Béchamp process involves stoichiometric reagents (iron and hydrochloric acid[52]) and does not meet green chemistry principle #9 (Table 1). As a first step (I in Tables 1 and 3), we have considered the catalytic reaction in batch liquid phase, which is standard practice in the pharmaceutical/chemical sector,[53] taking Pd/C as a benchmark catalyst. A representative (P_{H_2} = 5 atm) *o*-CNB concentration profile is shown in Figure 2(I,A), where complete conversion was achieved after 1 h. Selectivity (S_i) was time invariant with the generation of *o*-CAN as principal product ($S_{o\text{-CAN}}$ = 79%), AN as byproduct (S_{AN} = 20%), and trace NB formation (S_{NB} = 1%). An increase in pressure (to P_{H_2} = 12 atm) served to elevate the rate of *o*-CNB consumption with a measurable increase in *o*-CAN selectivity at the expense of AN (Table 3). As the same product distribution was obtained at all levels of conversions, *o*-CAN and AN must be generated in a parallel conversion of *o*-CNB rather than a stepwise hydrogenation/hydrodechlorination. There is evidence in the literature suggesting that selectivity in CNB hydrogenation is sensitive to P_{H_2}, where an increase in pressure (1−40 atm) favored CAN formation over (titania[54] and polymer[50]) supported Pt[50] and Pt−Au.[54] This was explained on the basis of a zero order

dx.doi.org/10.1021/sc500544s | ACS Sustainable Chem. Eng. 2014, 2, 2781−2789

dependence of hydrodechlorination (CAN → AN) on P_{H_2}, where an increase in P_{H_2} only affected *p*-CNB → *p*-CAN.[50] Batch reaction over Pd/C was accompanied by a lower E-factor (10) relative to the Béchamp process (15). Byproduct (AN and NB) formation contravenes principles #1, 2, 10, and 11 (Table 1), and process sustainability requires minimization of unwanted side reactions with enhanced atom efficiency, circumventing separation/purification steps. This objective was not achieved over the commercial Pd/C catalyst and was the focus of further optimization.

Second Approach to Optimisation: Batch Liquid Phase Operation over Au/TiO$_2$. The performance of Au/TiO_2 was tested in the batch reactor under conditions employed for Pd/C, and the results are presented in Figure 2(I,B) and Table 3. Full *o*-CNB conversion over Au/TiO_2 required an extended reaction time (up to 30 h), and the rate was appreciably lower (by a factor of more than 200 at P_{H_2} = 5 atm) than recorded for Pd/C. This can be ascribed to the lesser capacity of supported Au (relative to Pd) to adsorb/dissociate H_2, as demonstrated by the chemisorption measurements (Table 2). Ide et al.[55] reported lower (100−400 fold) hydrogenation rates for Au/C relative to Pd/C in the liquid phase conversion of crotonaldehyde and methyl vinyl ketone. However, Au/TiO_2 delivered 100% selectivity to *o*-CAN, where an increase in H_2 pressure elevated (selective) the hydrogenation rate to a greater extent than observed for Pd/C (Table 3). We can attribute this to a pressure-driven increase in the availability of surface hydrogen on Au/TiO_2 that enhanced the degree of hydrogenation. Use of Au/TiO_2 in batch mode lowered the E-factor to 8, which is at the lower end of the range (5−50) in the fine chemical sector.[56] Moreover, the ultraselective response over Au/TiO_2 satisfies five (#1, 2, 9, 10, and 11) of the green chemistry principles (Table 1). On the basis of this response, Au/TiO_2 was employed as catalyst for further process optimization. Full selectivity to the target product at elevated P_{H_2} translates into a higher *o*-CAN production rate, but this is offset by the energy required to operate the reactor (principle #6), notwithstanding the safety concerns associated with handling pressurized H_2, particularly at a commercial scale (principles #3 and #12). These drawbacks were tackled in the next optimization step.

Third Approach to Optimisation: Continuous Gas Phase Operation over Au/TiO$_2$. A move from batch liquid to continuous gas phase catalysis was made at the same reaction temperature (423 K) but at ambient pressure, lowering energy requirements and minimizing potential safety hazards. Continuous processing has been highlighted as crucial for sustainable manufacture of fine chemicals and a primary area for development by the Green Chemistry Institute (GCI), American Chemical Society (ACS), and global pharmaceutical corporations.[53,57] The feed was vaporised and carried through a fixed catalyst bed. This has the advantage of simultaneous reactant delivery and product removal where the process was operated at steady state. Representative temporal conversion profiles (Figure 2(II,A)) establish invariant activity for up to 3 h on-stream. We have previously established[58] applicability of pseudo-first-order kinetics according to

$$\ln\left[\frac{1}{(1-x)}\right] = k\left(\frac{n}{F}\right) \qquad (6)$$

where *n*/*F* (molar Au to inlet hourly *o*-CNB molar feed rate) has the physical significance of contact time. The linear relationship (between $\ln(1-x)^{-1}$ and *n*/*F*) shown in the inset to Figure 2(II,A) confirms adherence to first-order behavior, which allows determination of the rate constant (*k*). Catalyst lifetime is crucial where overall process efficiency is governed by both selectivity and stability.[59] Catalyst deactivation in $-NO_2$ group reduction has been ascribed to carbon deposition,[60] deleterious effects due to water formation (as byproduct),[61] chlorine poisoning,[58] and metal sintering.[58] Catalyst testing was extended over prolonged (up to 140 h) time on-stream where the results presented in Figure 2(II,B) demonstrate maintenance of constant activity. As a further test, contact time was increased (*n*/*F* from 0.08 to 0.34 h) during the stability measurements with a corresponding increase in conversion (to deliver 100% *o*-CAN yield) with a return to the initial level on switching back to the starting conditions (inset (a), Figure 2(II,B)). Reaction exclusivity in continuous gas phase operation resulted in an equivalent E-factor (= 8) to that obtained in liquid phase operation (Table 1). However, continuous operation overcomes the drawback of unproductive "down time" between batches, while operation of a fixed catalyst bed in continuous mode circumvents catalyst loss between batches, which was experimentally determined to be 5% per batch. This has a significant impact on productivity as can be assessed from the entries in Table 3. A meaningful comparison of both modes of operation should normalize *o*-CAN generated with respect to total process time to give a production capacity.[62] Liquid phase reaction was run in time-sequential steps (three recharges per week) with significant intervals between batches due to reactor loading (t_1), catalyst activation (t_2), temperature/pressure stabilization (t_3), extraction of product/recharge with reactant (t_4), and catalyst filtration−washing−reloading (t_5). Down time ($t_1 + t_2 + t_3$) in gas phase operation was limited due to combined (a) continuous reactant supply and product removal and (b) facile separation of catalyst from reactant/product. Productivities were calculated on the basis of 7 working (24 h) days per week where the estimated capacity (projected on an annual basis) was significantly greater for continuous operation (Table 3). The move from batch to continuous mode served to further close the sustainability gap, addressing nine green chemistry principles (Table 1) while increasing production capacity of the target amine.

Fourth Approach to Optimisation: Use of Water as Carrier in Continuous Gas Phase Operation over Au/TiO$_2$. The catalytic data presented to this point refer to reactions of ethanolic *o*-CNB solutions. Green chemistry requires, where possible, the use of "clean" solvents in tandem with milder conditions. Water, as an environmentally benign solvent, is a cleaner and inexpensive alternative, and the feasibility of conducting reactions in water rather than organic solvents has been a long-standing goal for synthetic chemists.[63] It has been demonstrated[14,64] that polar properties of water impact hydrogenation activity/selectivity in liquid phase reactions, but the effect in gas phase operation (where water serves as a carrier) has not been evaluated. Catalyst performance in gas phase hydrogenation can be influenced by the carrier due to competitive adsorption.[65] Use of water and water/ethanol mixtures was examined, and the results (inset (b), Figure 2(II,B) establish that rate increased markedly at higher water content; full selectivity to *o*-CAN was again achieved. Ning et al.[14] have reported enhanced *p*-CNB reduction over Ru/SiO_2

using water as solvent in comparison with organic alcohols (methanol to pentanol) in liquid phase reaction, which they attributed to a facilitated desorption of the halo-amine product. Maity et al.[64] observed increased activity in liquid phase hydrogenation of nitrobenzene over Pt/polymer in water relative to methanol, which was ascribed to more favorable formation of catalytic active sites in aqueous media. The hydrogenation rate over supported Au is limited by the available surface reactive hydrogen,[46] and any additional supply of hydrogen should promote reaction. Dissociative chemisorption of water on supported Au has been proposed under conditions similar to those used in this study, which served to increase activity in the water−gas shift reaction (WGSR)[66−68] and gas phase hydrogenation of benzaldehyde.[69] Shekhar et al.[67] have demonstrated that TiO_2 as Au support contributes directly to WGSR by activating water in the feed to generate surface reactive hydrogen. The generation of surface hydrogen (protons) from water dissociation is promoted by oxygen vacancies on TiO_2.[70] The abstracted protons can bond with two-coordinate oxygen sites on the support to form bridging hydroxyl groups that have been proposed as a source of atomic hydrogen, active in hydrogenation.[71] Theoretical calculations have established that the dissociation energy of water on Au sites is in the range 0.61−2.2 eV, which is of the same magnitude as the dissociative adsorption of hydrogen on Au (0.16−1.4 eV).[72−74] Enhanced selective hydrogenation of the aqueous *o*-CNB feed can then be ascribed to surface activation/dissociation of water, generating reactive hydrogen that contributes to $-NO_2$ reduction. Utilization of water as carrier resulted in further reduction in the E-Factor to 0.28 (Table 1), characteristic of highly optimized chemical processes in chemical/pharmaceutical production lines.[3] This is step-changing in fine chemical processes and is closer to the low waste/product ratios achieved in oil refining.[56] The increased rate in water resulted in further appreciable enhancement of *o*-CAN productivity (Table 3) and opens new opportunities for cleaner high-throughput production of functionalized aromatic amines.

AUTHOR INFORMATION

Corresponding Author

*E-mail: M.A.Keane@hw.ac.uk. Tel.: +44(0)131 451 4719.

Notes

The authors declare no competing financial interest.

REFERENCES

(1) Epicoco, M.; Oltra, V.; Jean, M. S. Knowledge dynamics and sources of eco-innovation: Mapping the green chemistry community. *Technol. Forecast. Soc. Change* **2014**, *81*, 388−402.

(2) Leahy, D. K.; Tucker, J. L.; Mergelsberg, I.; Dunn, P. J.; Kopach, M. E.; Purohit, V. C. Seven important elements for an effective green chemistry program: An IQ consortium perspective. *Org. Process Res. Dev.* **2013**, *17*, 1099−1109.

(3) Sanderson, K. It's not easy being green. *Nature* **2011**, *469*, 18−20.

(4) Tian, J.; Guo, Q.; Chen, Y.; Li, X.; Shi, H.; Chen, L. Study on industrial metabolism of carbon in a Chinese fine chemical industrial park. *Environ. Sci. Technol.* **2013**, *47*, 1048−1056.

(5) Anastas, P.; Eghbali, N. Green chemistry: Principles and practice. *Chem. Soc. Rev.* **2010**, *39*, 301−312.

(6) Anastas, P. T.; Warner, J. C. *Green Chemistry: Theory and Practice*; Oxford University Press: New York, 2000.

(7) Gawande, M. B.; Branco, P. S. An efficient and expeditious fmoc protection of amines and amino acids in aqueous media. *Green Chem.* **2011**, *13*, 3355−3359.

(8) Blaser, H. U.; Steiner, H.; Studer, M. Selective catalytic hydrogenation of functionalized nitroarenes: An update. *ChemCatChem.* **2009**, *1*, 210−221.

(9) Xiao, C.; Wang, X. D.; Lian, C.; Liu, H. Q.; Liang, M. H.; Wang, Y. Selective hydrogenation of halonitrobenzenes. *Curr. Org. Chem.* **2012**, *16*, 280−296.

(10) Cybulski, A.; Moulijn, J. A.; Sharma, M. M.; Sheldon, R. A. *Fine Chemicals Manufacture: Technology and Engineering*, 1st ed.; Elsevier: Amsterdam, 2001; p 564.

(11) Zuo, B.; Wang, Y.; Wang, Q.; Zhang, J.; Wu, N.; Peng, L.; Gui, L.; Wang, X.; Wang, R.; Yu, D. An efficient ruthenium catalyst for selective hydrogenation of *ortho*-chloronitrobenzene prepared *via* assembling ruthenium and tin oxide nanoparticles. *J. Catal.* **2004**, *222*, 493−498.

(12) Liu, M.; Yu, W.; Liu, H. Selective hydrogenation of *o*-chloronitrobenzene over polymer-stabilized ruthenium colloidal catalysts. *J. Mol. Catal. A: Chem.* **1999**, *138*, 295−303.

(13) Pietrowski, M.; Wojciechowska, M. An efficient ruthenium-vanadium catalyst for selective hydrogenation of *ortho*-chloronitrobenzene. *Catal. Today* **2009**, *142*, 211−214.

(14) Ning, J.; Xu, J.; Liu, J.; Miao, H.; Ma, H.; Chen, C.; Li, X.; Zhou, L.; Yu, W. A remarkable promoting effect of water addition on selective hydrogenation of *p*-chloronitrobenzene in ethanol. *Catal. Commun.* **2007**, *8*, 1763−1766.

(15) Zhang, G.; Wang, L.; Shen, K.; Zhao, D.; Freeman, H. S. Hydrogenation of *o*-chloronitrobenzene on a Pd/C catalyst doped with metal oxide nanoparticles. *Chem. Eng. J.* **2008**, *141*, 368−374.

(16) Irfan, M.; Glasnov, T. N.; Kappe, C. O. Heterogeneous catalytic hydrogenation reactions in continuous-flow reactors. *ChemSusChem* **2011**, *4*, 300−316.

(17) Shirvill, L. C.; Roberts, T. A.; Royle, M.; Willoughby, D. B.; Gautier, T. Safety studies on high-pressure hydrogen vehicle refuelling stations: Releases into a simulated high-pressure dispensing area. *Int. J. Hydrogen Energy* **2012**, *37*, 6949−6964.

(18) Cárdenas-Lizana, F.; Keane, M. A. The development of gold catalysts for use in hydrogenation reactions. *J. Mater. Sci.* **2013**, *48*, 543−564.

(19) Li, J.; Shi, X.-Y.; Bi, Y.-Y.; Wei, J.-F.; Chen, Z.-G. Pd nanoparticles in ionic liquid brush: A highly active and reusable heterogeneous catalytic assembly for solvent-free or on-water hydrogenation of nitroarene under mild conditions. *ACS Catal.* **2011**, *1*, 657−664.

(20) Perret, N.; Wang, X.; Onfroy, T.; Calers, C.; Keane, M. A. Selectivity in the gas-phase hydrogenation of 4-nitrobenzaldehyde over supported Au catalysts. *J. Catal.* **2014**, *309*, 333−342.

(21) Madon, R. J.; Boudart, M. Experimental criterion for the absence of artifacts in the measurement of rates of heterogeneous catalytic reactions. *Ind. Eng. Chem. Fundam.* **1982**, *21*, 438−447.

(22) Gómez-Quero, S.; Cárdenas-Lizana, F.; Keane, M. A. Effect of metal dispersion on the liquid phase hydrodechlorination of 2,4-dichlorophenol over Pd/Al_2O_3. *Ind. Eng. Chem. Res.* **2008**, *47*, 6841−6853.

(23) Ettireddy, P. R.; Ettireddy, N.; Mamedov, S.; Boolchand, P.; Smirniotis, P. G. Surface characterization studies of TiO_2 supported manganese oxide catalysts for low temperature SCR of NO with NH_3. *Appl. Catal., B* **2007**, *76*, 123−134.

(24) Ilieva, L.; Sobczak, J. W.; Manzoli, M.; Su, B. L.; Andreeva, D. Reduction Behavior of Nanostructured gold catalysts supported on mesoporous titania and zirconia. *Appl. Catal., A* **2005**, *291*, 85−92.

(25) Cárdenas-Lizana, F.; Gómez-Quero, S.; Perret, N.; Keane, M. A. Gold catalysis at the gas-solid interface: Role of the support in determining activity and selectivity in the hydrogenation of *m*-dinitrobenzene. *Catal. Sci. Technol.* **2011**, *1*, 652−661.

(26) Liu, S. Y.; Yang, S. M. Complete oxidation of 2-propanol over gold-based catalysts supported on metal oxides. *Appl. Catal., A* **2008**, *334*, 92−99.

(27) Hugon, A.; Delannoy, L.; Louis, C. Supported gold catalysts for the selective hydrogenation of 1,3-butadiene in the presence of an excess of alkenes. *Gold Bull.* **2008**, *41*, 127−138.

(28) Wang, X.; Perret, N.; Keane, M. A. Gas phase hydrogenation of nitrocyclohexane over supported gold catalysts. *Appl. Catal., A* **2013**, *467*, 575−584.
(29) Xiong, J.; Chen, J. X.; Zhang, J. Y. Liquid-phase hydrogenation of *o*-chloronitrobenzene over supported nickel catalysts. *Catal. Commun.* **2007**, *8*, 345−350.
(30) Yu, J.; Yu, H.; Cheng, B.; Zhou, M.; Zhao, X. Enhanced photocatalytic activity of TiO_2 powder (P25) by hydrothermal treatment. *J. Mol. Catal. A: Chem.* **2006**, *253*, 112−118.
(31) Bickley, R. I.; Gonzalez-Carreno, T.; Lees, J. S.; Palmisano, L.; Tilley, R. J. D. A structural investigation of titanium dioxide photocatalysts. *J. Solid State Chem.* **1991**, *92*, 178−190.
(32) Kim, D. H.; Chin, Y.-H.; Muntean, G. G.; Yezeretz, A.; Currier, N. W.; Epling, W. S.; Chen, H.-Y.; Hess, H.; Peden, C. H. F. Relationship of Pt particle size to the NO_x storage performance of thermally aged $Pt/BaO/Al_2O_3$ lean NO_x trap catalysts. *Ind. Eng. Chem. Res.* **2006**, *45*, 8815−8821.
(33) Corma, A.; Boronat, M.; González, S.; Illas, F. On the activation of molecular hydrogen by gold: A theoretical approximation to the nature of potential active sites. *Chem. Commun.* **2007**, *32*, 3371−3373.
(34) Bus, E.; Miller, J. T.; van_Bokhoven, J. A. Hydrogen chemisorption on Al_2O_3-supported gold catalysts. *J. Phys. Chem. B* **2005**, *109*, 14581−14587.
(35) Cárdenas-Lizana, F.; Gómez-Quero, S.; Perret, N.; Keane, M. A. Support effects in the selective gas phase hydrogenation of *p*-chloronitrobenzene over gold. *Gold Bull.* **2009**, *42*, 124−132.
(36) Cárdenas-Lizana, F.; Gómez-Quero, S.; Idriss, H.; Keane, M. A. Gold particle size effects in the gas-phase hydrogenation of *m*-dinitrobenzene over Au/TiO_2. *J. Catal.* **2009**, *268*, 223−234.
(37) Lin, S.; Vannice, M. A. Gold dispersed on TiO_2 and SiO_2: Adsorption properties and catalytic behavior in hydrogenation reactions. *Catal. Lett.* **1991**, *10*, 47−62.
(38) Amorim, C.; Yuan, G.; Patterson, P. M.; Keane, M. A. Catalytic hydrodechlorination over Pd supported on amorphous and structured carbon. *J. Catal.* **2005**, *234*, 268−281.
(39) Shi, C.; Jang, B. W.-L. Nonthermal RF plasma modifications on $Pd/\gamma\text{-}Al_2O_3$ for selective hydrogenation of acetylene in the presence of ethylene. *Ind. Eng. Chem. Res.* **2006**, *45*, 5879−5884..
(40) Ferrer, V.; Moronta, A.; Sánchez, J.; Solano, R.; Bernal, S.; Finol, D. Effect of the reduction temperature on the catalytic activity of Pd-supported catalysts. *Catal. Today* **2005**, *107*−*108*, 487−492.
(41) Mendez, C. M.; Olivero, H.; Damiani, D. E.; Volpe, M. A. On the role of Pd β-hydride in the reduction of nitrate over Pd based catalyst. *Appl. Catal., B* **2008**, *84*, 156−161.
(42) Cárdenas-Lizana, F.; Hao, Y.; Crespo-Quesada, M.; Yuranov, I.; Wang, X.; Keane, M. A.; Kiwi-Minsker, L. Selective gas phase hydrogenation of *p*-chloronitrobenzene over Pd catalysts: Role of the support. *ACS Catal.* **2013**, *3*, 1386−1396.
(43) Li, G.; Jiang, L.; Jiang, Q.; Wang, S.; Sun, G. Preparation and characterization of Pd_xAg_y/C electrocatalysts for ethanol electro-oxidation reaction in alkaline media. *Electrochim. Acta* **2011**, *56*, 7703−7711.
(44) Prelazzi, G.; Cerboni, M.; Leofanti, G. Comparison of H_2 adsorption, O_2 adsorption, H_2 titration, and O_2 titration on supported palladium catalysts. *J. Catal.* **1999**, *181*, 73−79.
(45) Greeley, J.; Mavrikakis, M. Surface and subsurface hydrogen: Adsorption properties on transition metals and near-surface alloys. *J. Phys. Chem. B* **2005**, *109*, 3460−3471.
(46) Wang, X.; Perret, N.; Keane, M. A. The role of hydrogen partial pressure in the gas phase hydrogenation of *p*-chloronitrobenzene over alumina supported Au and Pd: A consideration of reaction thermodynamics and kinetics. *Chem. Eng. J.* **2012**, *210*, 103−113.
(47) Cárdenas-Lizana, F.; Gómez-Quero, S.; Keane, M. A. Clean production of chloroanilines by selective gas phase hydrogenation over supported Ni catalysts. *Appl. Catal., A* **2008**, *334*, 199−206.
(48) Wang, X. D.; Liang, M. H.; Zhang, J. L.; Wang, Y. Selective hydrogenation of aromatic chloronitro compounds. *Curr. Org. Chem.* **2007**, *11*, 299−314.
(49) Zhao, B.; Chen, Y.-W. The effect of poly-n-vinylpyrrolidone modification on NiCoB catalysts for hydrogenation of *p*-chloronitrobenzene. *Mater. Chem. Phys.* **2011**, *125*, 763−768.
(50) Cárdenas-Lizana, F.; Berguerand, C.; Yuranov, I.; Kiwi-Minsker, L. Chemoselective hydrogenation of nitroarenes: Boosting nanoparticle efficiency by confinement within highly porous polymeric framework. *J. Catal.* **2013**, *301*, 103−111.
(51) Coq, B.; Tijani, A.; Dutartre, R.; Figuéras, F. Influence of support and metallic precursor on the hydrogenation of *p*-chloronitrobenzene over supported platinum catalysts. *J. Mol. Catal.* **1993**, *79*, 253−264.
(52) Popat, V.; Padhiyar, N. Kinetic study of bechamp process for *p*-nitrotoluene reduction to *p*-toluidine. *Int. J. Chem. Eng. Appl.* **2013**, *4*, 401−405.
(53) Wiles, C.; Watts, P. Continuous flow reactors: A perspective. *Green Chem.* **2012**, *14*, 38−54.
(54) He, D. P.; Jiao, X. D.; Jiang, P.; Wang, J.; Xu, B. Q. An exceptionally active and selective $Pt\text{-}Au/TiO_2$ catalyst for hydrogenation of the nitro group in chloronitrobenzene. *Green Chem.* **2012**, *14*, 111−116.
(55) Ide, M. S.; Hao, B.; Neurock, M.; Davis, R. J. Mechanistic insights on the hydrogenation of α,β-unsaturated ketones and aldehydes to unsaturated alcohols over metal catalysts. *ACS Catal.* **2012**, *2*, 671−683.
(56) Sheldon, R. A. The E factor: Fifteen years on. *Green Chem.* **2007**, *9*, 1273−1283.
(57) Jiménez-González, C.; Poechlauer, P.; Broxterman, Q. B.; Yang, B.-S.; am_Ende, D.; Baird, J.; Bertsch, C.; Hannah, R. E.; Dell'Orco, P.; Noorrnan, H.; Yee, S.; Reintjens, R.; Wells, A.; Massonneau, V.; Manley, J. Key green engineering research areas for sustainable manufacturing: A perspective from pharmaceutical and fine chemicals manufacturers. *Org. Process Res. Dev.* **2011**, *15*, 900−911.
(58) Wang, X.; Perret, N.; Delgado, J. J.; Blanco, G.; Chen, X.; Olmos, C. M.; Bernal, S.; Keane, M. A. Reducible support effects in the gas phase hydrogenation of *p*-chloronitrobenzene over gold. *J. Phys. Chem. C* **2013**, *117*, 994−1005.
(59) Moulijn, J. A.; van_Diepen, A. E.; Kapteijn, F. Catalyst deactivation: Is it predictable?: What to do? *Appl. Catal., A* **2001**, *212*, 3−16.
(60) Cárdenas-Lizana, F.; Wang, X.; Lamey, D.; Li, M.; Keane, M. A.; Kiwi-Minsker, L. An examination of catalyst deactivation in nitroarene hydrogenation over supported gold. *Chem. Eng. J.* **2014**, *255*, 695−704.
(61) Sangeetha, P.; Seetharamulu, P.; Shanthi, K.; Narayanan, S.; Rama Raob, K. S. Studies on Mg-Al oxide hydrotalcite supported pd catalysts for vapor phase hydrogenation of nitrobenzene. *J. Mol. Catal. A: Chem.* **2007**, *273*, 244−249.
(62) Goršek, A.; Glavič, P. Design of batch versus continuous processes: Part I: Single-purpose equipment. *Chem. Eng. Res. Des.* **1997**, *75*, 709−717.
(63) Sharma, U.; Verma, P. V.; Kumar, N.; Kumar, V.; Bala, M.; Singh, B. Phosphane-free green protocol for selective nitro reduction with an iron-based catalyst. *Chem.—Eur. J.* **2011**, *17*, 5903−5904.
(64) Maity, P.; Basu, S.; Bhaduri, S.; Lahiri, G. K. Superior performance of a nanostructured platinum catalyst in water: Hydrogenations of alkenes, aldehydes and nitroaromatics. *Adv. Synth. Catal.* **2007**, *349*, 1955−1962.
(65) Augustine, R. L.; Warner, R. W.; Melnick, M. J. Heterogeneous catalysis in organic chemistry. 3. Competitive adsorption of solvents during alkene hydrogenations. *J. Org. Chem.* **1984**, *49*, 4853−4856.
(66) Gong, J. Structure and surface chemistry of gold-based model catalysts. *Chem. Rev.* **2011**, *112*, 2987−3054.
(67) Shekhar, M.; Wang, J.; Lee, W.-S.; Williams, W. D.; Kim, S. M.; Stach, E. A.; Miller, J. T.; Delgass, W. N.; Ribeiro, F. H. Size and support effects for the water−gas shift catalysis over gold nanoparticles supported on model Al_2O_3 and TiO_2. *J. Am. Chem. Soc.* **2012**, *134*, 4700−4708.

(68) Burch, R. Gold catalysts for pure hydrogen production in the water-gas shift reaction: Activity, structure and reaction mechanism. *Phys. Chem. Chem. Phys.* **2006**, *8*, 5483−5500.
(69) Li, M.; Wang, X.; Perret, N.; Keane, M. A. Enhanced production of benzyl alcohol in the gas phase continuous hydrogenation of benzaldehyde over Au/Al_2O_3. *Catal. Commun.* **2014**, *46*, 187−191.
(70) Oviedo, J.; Sanchez de-Armas, R.; San Miguel, M. A.; Sanz, J. F. Methanol and water dissociation on TiO_2 (110): The role of surface oxygen. *J. Phys. Chem. C* **2008**, *112*, 17737−17740.
(71) Buchanan, D. A.; Webb, G. Catalysis by group IB metals 1: Reaction of buta-1,3-diene with hydrogen and with deuterium catalyzed by alumina-supported gold. *J. Chem. Soc., Faraday Trans.* **1975**, *71*, 134−144.
(72) Fajin, J. L. C.; Cordeiro, M.; Gomes, J. R. B. Cluster and periodic DFT calculations of adsorption of hydroxyl on the Au(hkl) surfaces. *J. Mol. Struct.* **2010**, *946*, 51−56.
(73) Wang, G.-C.; Tao, S.-X.; Bu, X.-H. A systematic theoretical study of water dissociation on clean and oxygen-preadsorbed transition metals. *J. Catal.* **2006**, *244*, 10−16.
(74) Zanchet, A.; Dorta-Urra, A.; Roncero, O.; Flores, F.; Tablero, C.; Paniagua, M.; Aguado, A. Mechanism of molecular hydrogen dissociation on gold chains and clusters as model prototypes of nanostructures. *Phys. Chem. Chem. Phys.* **2009**, *11*, 10122−10131.